Proceedings of the Institution of Mechanical Engineers, Part E: Journal of Process Mechanical Engineering

https://journals.sagepub.com/home/pie

Impact factor = 1.620

(Accepted September 24th 2021)

Augmentation of Heat Transfer via Nanofluids in Duct Flows using Fourier-Type Conditions: Theoretical and Numerical Study

J.C. Umavathi

Professor of Applied Mathematics, Department of Mathematics, Gulbarga University, Gulbarga-585 106, Karnataka, ***India. Email:*** *drumavathi@rediffmail.com*

O. Anwar Bég

Professor of Engineering Science, Aeronautical/Mechanical Engineering Dept., School of Science, Engineering and Environment (SEE), Salford University, Manchester, M54WT, ***UK****.*

Email*: O.A.Beg@salford.ac.uk*

ABSTRACT:

Motivated by developments in thermal duct processing, an investigation is presented to study the behavior of viscous nanoparticle suspensions flowing in a vertical duct subject to *Fourier-type* conditions. The left wall temperature is kept lower than that of the right wall. Brownian motion and thermophoresis which are invoked via the presence of nanoparticles are incorporated in the study. Implementing suitable transformations, the balance equations are rendered in dimensionless form. These non-linear and coupled conservation equations for momentum, heat and nanoparticle concentration are solved with appropriate boundary conditions using a regular perturbation method for low values of emerging parameters. Numerical solutions with an efficient Runge-Kutta shooting method, are also presented at all values of the control parameters. The impact of thermal Grashof number $(0 \le \Lambda \le 15)$, Eckert number $(0.01 \le Ec \le 0.04)$, and thermophoresis $(0.05 \le Nt \le 2)$ and Brownian motion parameters $(0.05 \le Nt \le 2)$, on the velocity, temperature and nanoparticle concentration distributions for

identical $\left(Bi_1 = Bi_2 = 10\right)$ and differing Biot numbers $\left(Bi_1 = 1,\ Bi_2 = 10\right)$ (at the duct walls) are computed and visualized graphically. With vanishing thermophoresis and Brownian motion parameters, the solutions match exactly with the earlier Newtonian viscous flow computations. Symmetric and asymmetric wall heat conditions are also acknowledged. Intensifying the thermal Grashof number, Eckert number, thermophoresis parameter and Brownian parameter serves to amplify magnitudes of the velocity and temperature whereas the nanoparticle concentration field is suppressed. The skin friction and Sherwood number are also computed with various combinations of the flow control parameters. Nusselt number values at the hot duct wall, are enhanced with an increment in thermal buoyancy parameter, Eckert number, Brownian motion parameter and thermophoresis parameter for equal Biot numbers. The opposite trend is computed for different Biot numbers. For any given values of Biot numbers, the mean velocity and bulk temperature are boosted with increment in thermal buoyancy parameter, Eckert number, Brownian motion parameter and thermophoresis parameter. Hence it may be inferred that the transport characteristics computed using *Fourier type* boundary conditions are substantially different from those based on isothermal boundary conditions in nanofluid duct flows.

KEYWORDS: *Nanofluids, Convective boundary conditions, Perturbation Solutions, Thermal duct flows, Fourier conditions, Runge-Kutta Shooting method, Dissipation, Nusselt number, Sherwood number.*

NOMENCLATURE:

A	Constant $\left[Pa\ m^{-1}\right]$
$Bi_1,\ Bi_2$	Biot Numbers at the duct walls [-]
Br	Brinkman number [-]
Cp	Isobaric specific heat (constant pressure) [J/K]
C_f	Skin friction coefficient [Moles/m^3]
C_0	Reference nanoparticle volume fraction [Moles/m^3]
C	nanoparticle volume fraction [Moles/m^3]
$C_1,\ C_2$	Nanoparticle volume fraction on the boundaries (duct walls) [Moles/m^3]
D_B	Brownian diffusion coefficient [-]

D_T	Thermophoretic diffusion coefficient [-]
$D(=2L)$	Hydraulic diameter $[m]$
Ec	Eckert number [-]
f	Dimensionless stream function [-]
g	Acceleration due to gravity $\left[ms^{-2}\right]$
GR_T	Grashof number $\left(g\beta\Delta TD^3/\nu^2\right)$ [-]
h_1, h_2	Convective heat transfer coefficients at the walls [W/(m^{2}K)]
k	Thermal conductivity [W/(mK)]
L	Channel width $[m]$
n	Non-negative integer number [-]
Nt	Thermophoresis parameter [-]
Nb	Brownian motion parameter [-]
Nu_1, Nu_2	Nusselt numbers at the duct walls [-]
p	Pressure $[Pa]$
$P = p + \rho_0 gX$	Hydrostatic pressure $[Pa]$
Pr	Prandtl number (ν/α) [-]
Re	Reynolds number $(U_0 D/\nu)$ [-]
R_T	Temperature difference ratio $\left((T_2 - T_1)/\Delta T\right)$ [-]
S	Dimensionless parameter [-]
T	Temperature $[K]$
T_0	Reference temperature [K]
T_1, T_2	Temperature at the hot duct walls [K]
T_∞	Ambient temperature [K]
u	Dimensionless velocity in the X-direction [-]
$u_n(y)$	Dimensionless functions [-]

$\bar{u}$	Mean value of u $\left[ms^{-1}\right]$
U	Dimensional velocity component in the X -direction $\left[ms^{-1}\right]$
U_0	Reference velocity $\left[ms^{-1}\right]$
y	Dimensionless transverse coordinate [-]
X	Streamwise coordinate $\left[m\right]$
Y	Transverse coordinate $\left[m\right]$

Greek Symbols

α	Thermal diffusivity $\left(K/\rho_0 c_0\right)\left[m^2 s^{-1}\right]$
β_T	Thermal expansion coefficient $\left[K^{-1}\right]$
ΔT	Reference temperature difference [K]
ΔC	Reference nanoparticle volume fraction difference [Moles/m^3]
τ_1, τ_2	Skin friction components [N/m^2]
τ	Skin friction [N/m^2]
ε	Dimensionless perturbation parameter [-]
θ	Dimensionless temperature [-]
θ_b	Dimensionless bulk temperature [-]
ϕ	Dimensionless nanoparticle volume fraction [-]
υ	Kinematic viscosity $\left(\mu/\rho_0\right)\left[m^2 s^{-1}\right]$
Λ	Thermal Grashof number $\left(GR_T/\mathrm{Re}\right)$[-]
μ	Dynamic viscosity [kg/(ms)]
$\left(\rho c\right)_p$	Heat capacity of the nanoparticle material [J/K]
$\left(\rho c\right)_f$	Heat capacity of the base fluid [J/K]
ρ_0	Mass density when $T=T_0$ [kg/m^3]

1. Introduction

Thermal convection is an important phenomenon in mechanical engineering and features extensively in many diverse applications including geothermal power, OTEC (ocean thermal energy conversion) plants, architectural ventilation systems, solar energy, materials processing, nuclear energy, fire propagation and thermal insulation. A major limitation against optimizing the energy transfer in engineering systems is the inherently poor thermal conductivity of conventional fluids, including oil, water and ethylene glycol mixture. Therefore, for more than a century since Maxwell's original work in 1873, scientists and engineers have made a great effort to break this fundamental limit by dispersing millimeter or micrometer sized particles in liquids. However, the major problem with the use of such large particles is the rapid sedimentation of these particles in fluids. Maxwell's concept, albeit old laid the foundation for new innovative developments in the late 20th century, specifically *nanofluids*. Nanofluids are colloidal suspensions which are synthesized by dispersing nanometer-sized particles in conventional base fluids, to create stable and highly conductive suspensions, which demonstrate improved dynamic thermal interactions. Recognizing an excellent opportunity to apply nanotechnology, Eastman *et al.* [1] pioneered the novel concept of nanofluids by hypothesizing that it is viable to break down these century-old technical barriers by exploiting the unique properties of nanoparticles. The original application area was automotive radiator systems but new areas including flame retardants[2], geothermal energy[3], aerospace fuels[4] , rheological materials processing[5] , tribology[6], thermal insulation systems[7] , commercial heat exchangers[8], biomedical pharmaceutics[9], petroleum drilling technology[10], solar technology[11], food manufacturing[12], coating protection systems, soft robotics, thermal engineering, environmental systems (remediation) and biomicrofluidics,[13] have also been explored using nanofluids.

Metallic or metallic oxide nanoparticles such as alumina, titania and copper oxide, unlike larger-sized particles, can be suspended stably within the fluids without settling out of suspension. Thus, these nanofluids avoid numerous problems such as abrasion, clogging and high-pressure loss, and are contemplated to be next-generation fluids in 21st century heat transfer technologies. The excellent thermal conductivity of nanofluids was verified experimentally by Massuda *et al.*[14]. Following their report, a substantial number of both experimental and theoretical publications on nanofluids emerged in the open literature in the last two decades –

see[15-18]. Cooling performance of a microchannel heat sink with nanofluids was presented by Jang and Choi[19] . Heris *et al.*[20] carried out experiment on convective heat transfer of Al_2O_3 / water nanofluid in a circular tube. Pak and Cho[21] researched on the hydrodynamic and heat transfer study of dispersed fluids with submicron metallic oxide particles. Experimental microchannel heat sink performance studies was carried out by Chein and Chuang[22] using nanofluids. Lee and Mudawar[23] assessed the effectiveness of nanofluids for single phase and two- phase heat transfer in microchannels. Heat transfer characteristics of nanofluids was studied and reviewed by . Dring *et al.*[24] and Wang and Mujumdar[25] respectively.

The theoretical investigation was explored by Hu *et al.*[26] on heat and mass transfer behavior of magnetohydrodynamic radiative Ferro fluid flow caused by a cone in the presence of source or sink. They concluded that the impact of Brownian motion parameter is less in $CoFe_2O_4$ + water at 50^0C when compared with $CoFe_2O_4$ +water at 10^0C and hence the mass transfer rate was high for $CoFe_2O_4$ at 50^0C. Also the heat source or sink parameter acted as a controlling parameter for the flow and also for the heat transport phenomena. Mahesh *et al.*[27] reported on the hybrid nanofluid for the influence of Reynolds number, stretching of lower and upper disks on the dynamics of water conveying grapheme and silver between rotating disks when Lorentz's force, Joule heating, suction, thermal radiation of thermal energy and Catteneo-Christov heat flux. They highlighted that increasing the Reynolds number improves the thermal field but reduces the tangential velocity. The entropy generation was an increasing property of stretching lower and upper disks but this were yardsticks for decreasing Bejan number. The finite element analysis of water-conveying iron (III) oxide and silver nanoparticles in a rectangular cavity mounted with two heat fins on the bottom wall subject to Buoyancy and Lorentz forces was investigated by Soumya *et al.*[28]. Their analysis claimed that the lower Rayleigh number and higher Hartman number caused for the laminar flow whereas higher Rayleigh number and lower Hartman number resulted in the turbulent flow. Also by increasing the length and width of the fins led for the intense velocity profiles, stream line function and increased the temperature.

Nehad *et al.*[29] examined the significance of increasing radius of nanoparticles, energy flux due to concentration gradient and mass flux due to temperature gradient in the dynamics of chemically reactive fluid subject to suction and inclined magnetic strength. They pointed that

the velocity was enhanced with the reduction in the viscosity of water based nanofluid due to a higher radius of copper nanoparticles. Significance reduction in temperature was attained across the domain due to increasing radius of copper nanoparticles when energy flux due to concentration gradient was sufficiently large. Thanaa *et al*.[30] also researched the signification of of suction and dual-stretching on three-dimensional flow of water conveying nanoparticles with various shapes and densities using ternary-hybrid nanofluids. Nehad *et al*.[31] examined the dynamics of hybrid nanofluids using type-I and type-II hybrid models with emphasis on the difference. They found that the local skin friction coefficient and temperature coefficient are decreasing property of suction. Using seven different hybrid nanofluids with base fluid as water, the optimal Nusselt number was attained at a larger value of stretching ratio and suction.

Although nanofluids are solid-liquid mixtures, the approach adopted conventionally in most mathematical modeling studies is to simulate the nanofluid as a *single-phase* (homogenous) fluid. In fact, irrespective of the extreme size and low concentration of the dispersed nanaoparticles, the particles are assumed to move with the same velocity as the base fluid. Also, by assuming *local thermal equilibrium*, the solid particle-liquid mixture may then be approximately considered to behave as a conventional single-phase fluid with properties that are to be evaluated as functions of those of the constituents.

Several authors have tried to establish convective transport models for nanofluids. A nanofluid is a two-phase mixture in which the solid phase consists of nano-sized particles. In view of nanoscale size, it may be questionable whether the *theory of two-phase flow* can be applied in describing nanofluid dynamics. On the other hand, several factors such as gravity, friction between the solid and fluid particles and Brownian forces, Brownian diffusion, sedimentation and dispersion, may substantially influence nanofluid transport phenomena. Consequently, the slip velocity between the particles and fluid cannot be neglected for simulating nanofluid flows.

Since the two-phase approach considers the movement between the solid and fluid molecules, it may provide improved predictions in nanofluid flow simulations. To fully describe and predict the flow and behavior of complex flows, different multiphase theories have been proposed and used. A large number of articles concerning multiphase flows have employed the *mixture theory* to predict the behavior of nanofluids[32-34]. Considerable progress was made by

Buongiorno[35] who carefully developed a theoretical analysis to estimate the relative magnitudes of the terms associated with all possible slip mechanisms, namely, inertia, Brownian diffusion, thermophoresis, diffusiophoresis, Magnus effect (lift of particles associated with circular motion), fluid drainage and gravity. However, in nanofluid convective transport phenomena only Brownian diffusion and thermophoresis were established as having a significant role. He derived a two-component four-equation model for nanofluids, which has been used by many researchers including Tzou[36,37] , Hwang *et al.*[38], Nield and Kuznetsov[39] and many others. Yet, there still exist some controversies as to specifically which particular conditions are amenable for nanoparticle heat transfer enhancement[40]. Furthermore, there is still an open debate pertaining to whether or not, the nanofluids convective heat transfer enhancement exceeds in a sustained fashion the base fluid thermal performance.

Gao and co-workers[41-43] first considered whether the effect of thermal conductivity increment may be dependent on the shape of nanoparticles. They also implemented an alternative theory with the help of Bruggeman's model to approximate the thermal conductivity of dispersion with *non-spherical* solid nanoparticles. Recently, with the help of Buongiorno's nanoscale formulation, the effect of local thermal non-equilibrium on the stability of nanofluid convective transport was investigated theoretically by Kim *et al.*[44] and Nield and Kuznetsov[45].

Omid *et al.*[46] conducted a study to determine the influences of perforated anchors on heat transfer intensification of turbulence nanofluid flow in a pipe. The conclusions drawn were that the thermal enhancement factor decreases as the Reynolds number decreased. The addition of nanoparticles increased the friction factor. At Re = 25, 000 the friction faction increased to 11.48% by adding the 5% of nanoparticles when compared with the base fluid without nanoparticles. Saeedreza *et al.*[47] simulated Al_2O_3-water nanofluid flow and forced convection around a rotating circular cylinder. The important results drawn by them was that there was an augmentation of heat transfer rate by adding the nanoparticles to the base fluid and reduction in drag coefficient by creating the rotation at Re = 100, and 0.05% nanoparticle concentration. Hence applying the nanoparticles in a rotating system enables the energy management at higher values of Reynolds number. For 0.05% nanoparticle concentration and for Reynolds number 5 and 100, the Nusslet number was reduced with increasing rotation rate to 6.9% and 32% respectively. Magnetohydrodynamic and Al_2O_3-water nanofluid flow around a vortex facing

triangular obstacle was discussed by Rashidi *et al.*[48]. The mail results concluded was that a stronger magnetic field was needed for vanishing the reciruculating wake and stabilizing the flow in nanofluid in comparision with regular fluid. The drag coefficient decreased with increased Stuart number. Further the impact of magnetic filed on reduction of heat transfer increased with increasing the concentration of nanoparticles.

Rashidi *et al.*[49] also discussed on the stuructural optimization of nanofluid flow around an equilateral triangular obstacle. Numerical and optimization techniques were used to determine the optimum thermal and flow condition for nanofluids around an equilateral obstacle. Their study markded that the drag coefficient and Nusselt number were sensitive to the orientation of obstacle rather than the solid volume fraction and Reynolds number. The minimum drag coefficient was occurred between the diagonal and vortex facing flows.

Mahla *et al.*[50] presented the two-way couple of Eulerian-Lagrangian model for particle transport with different sizes in an obstructed channel. The governing equations for flow and particle motions were solved by using Finite volume and trajectory anlysis. The highlights of the study was that the particle deposition percentage increased with increasing particle size, the thermophoresis effect on cross-steam particle velocity was negligible, the mass diffusion boundary layer grows along the channel and the nanometer particle does not follow the flow stream **line.** Mosoud *et al.*[51] analysed the flow of nanofluid in duct using Eulerian-Lagrangina model. The important finding were that, for the reflect boundary conditions, the concentration on nanoparticles were almost constant with slight change near the wall and the concentration profiles were nearly convergent to a single graph for low values of solid volume fraction (0.01%) and there were some deviation for high values (0.05%). There was a slight increase in the average Nusselt number for the reflect boundary conditions in comparison to trap boundary.

Boundary conditions can have a profound influence on thermophysical characteristics of many flow configurations including thermal ducts, enclosures, external boundary layers etc. The convective boundary condition also known as the *Newton/Robin boundary condition*, corresponds to the existence of convection heating (or cooling) at the surface (boundary). It is based on the energy Robin condition and is probably the most common boundary condition encountered in practice since most heat transfer surfaces are exposed to a convective environment under working conditions. In other words, this condition assumes that the heat

conduction at the exterior is equal to the thermal convection at the surface in the same direction. Since the boundary cannot store energy, the net heat entering the surface from the convective side must leave the surfaces from the conduction side. The Robin conditions set the values of a consolidation of the unknown function and its normal gradient. Other heat transfer problems in the literature – see Aung and Worku[52], Cheng *et al.*[53], Barletta[54], Grosan and Pop[55] etc. used *Neumann boundary conditions* for temperature. Limited authors such as Javeri[56] , Zanchini[57] have used the *Dirichlet boundary condition* on the temperature. Novy *et al.*[58], Bixler[59], Papanastasiou *et al.*[60] described analytically the influence of different types of wall conditions on temperature distributions in various convective flow regimes.

It was proven that the *Fourier-type condition* gives the most accurate solutions in convective heat transfer. Arturo *et al.*[61] studied the influence of Fourier-type, Dirichlet, and Neumann conditions on complex geometries using the immersed-boundary techniques. Umavathi and Bég[62, 63] implemented Robin boundary conditions for various thermophysical duct flows with multiple effects including porous media drag and chemical reactions. Recently, Jaewook *et al*[64] analyzed the thermal properties in rough channel forced convection flow observing that Robin–type effective boundary conditions quite adequately describe the effect of the rough layer on the heat transfer

In the present study, *dissipative nanofluid buoyancy-driven flow in a thermal duct is considered with Fourier-type boundary conditions which provide greater accuracy than Dirichlet and Neumann conditions*. The two-component Bungiorno nanoscale model[17] is implemented. The duct left wall temperature is kept lower than that of the right wall. The non-dimensional coupled conservation equations for momentum, heat and nanoparticle concentration are solved with appropriate boundary conditions using a regular perturbation method for low values of emerging parameters. Numerical solutions with an efficient Runge-Kutta shooting method, are also presented at all values of the control parameters. The influence of thermal Grashof number, Eckert number, thermophoresis and Brownian motion parameters, on the velocity, temperature and nanoparticle concentration distributions for identical and differing Biot numbers are computed and visualized graphically. Skin friction, Nusselt numbers and Sherwood numbers at both duct walls are also computed. Validation for vanishing nanoscale effects are included with the earlier study of Zanchini[57]. The work is relevant to improving thermal

performance in engineering duct systems[65], air conditioning systems[66], channel process operations in manufacturing[67, 68] and heat exchanger designs[69].

2. Mathematical formulation

Steady, two-dimensional, incompressible, laminar fully developed free convection flow in an open-ended vertical conduit (duct) as shown in **Fig. 1**. The X - axis is taken as vertically upward, and parallel to the direction of the buoyancy forces, and the Y -axis is normal to it. This vertical channel occupies the region $-L/2 \le Y \le L/2$ and it is maintained at a constant temperature. The properties of the nanofluid are constant and furthermore the nanoparticle concentration at the left duct wall is C_1 and at the right duct wall is C_2 with Fourier-type conditions. The thermal conductivity, thermal diffusivity, dynamic viscosity and thermal expansion coefficient of the nanofluid are fixed.

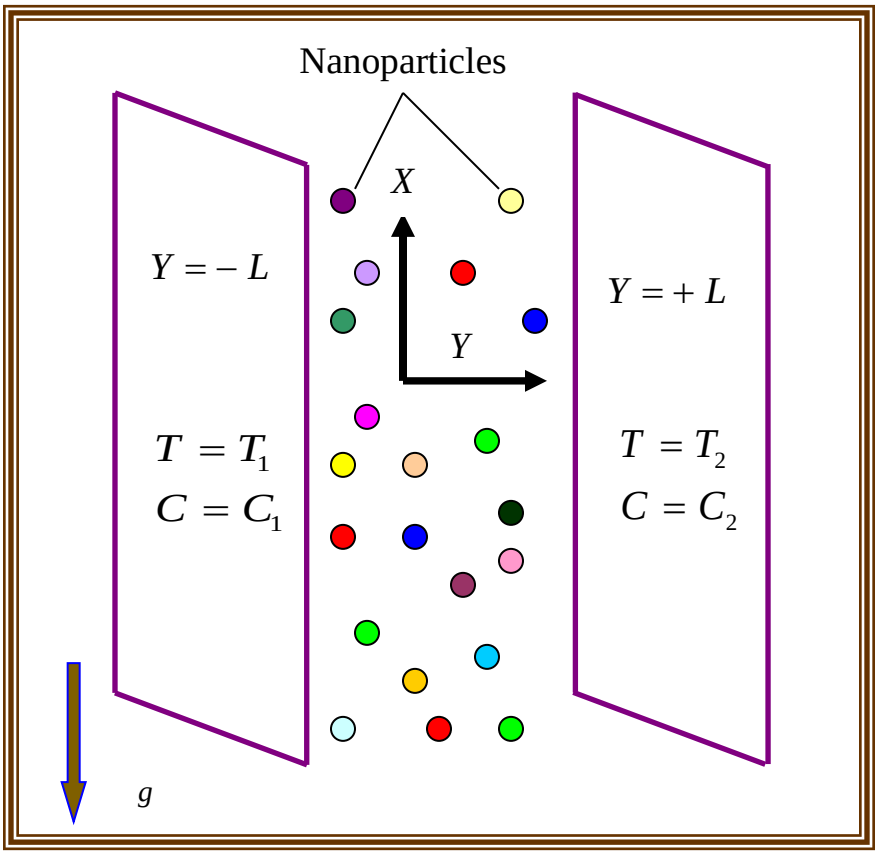

Figure 1. Physical configuration for nanofluid duct flow

The momentum balance equation takes the form (Zanchini[57]):

$$\beta_T g(T-T_0)-\frac{1}{\rho_0}\frac{\partial P}{\partial X}+\upsilon\frac{d^2U}{dY^2}=0 \tag{1}$$

In the presence of viscous dissipation, the heat (energy) balance equation can be written as: (Buongiorno[35])

$$\alpha\frac{d^2T}{dY^2}+\tau\left[D_B\left(\frac{\partial C}{\partial Y}\frac{\partial T}{\partial Y}\right)+\frac{D_T}{T_\infty}\left(\frac{\partial T}{\partial Y}\right)^2\right]+\frac{\upsilon}{C_P}\left(\frac{dU}{dY}\right)^2=0 \tag{2}$$

The nanoparticle volume fraction equation has the form: (Buongiorno[35])

$$D_B\frac{d^2C}{dY^2}+\frac{D_T}{T_\infty}\frac{d^2T}{dY^2}=0 \tag{3}$$

Here P is the pressure, υ is kinematic viscosity, $\tau=\rho C_p/\rho C_f$ is the ratio of nanoparticle heat capacity and the base fluid, α is the thermal diffusivity of the base fluid, D_T is the thermophoretic diffusion coefficient, D_B is the Brownian diffusion coefficient, T is the local temperature. The associated boundary conditions for the velocity field are imposed as:

$$u\left(-L/2\right)=u\left(L/2\right)=0 \tag{4}$$

For the temperature field, the boundary conditions are:

$$-k\left.\frac{\partial T}{\partial Y}\right|_{-L/2}=h_1[T_1-T(X,-L/2)] \tag{5}$$

$$-k\left.\frac{\partial T}{\partial Y}\right|_{L/2}=h_2[T(X,L/2)-T_2] \tag{6}$$

Finally, the boundary conditions for the nanoparticle volume fraction field are prescribed as:

$$C=C_1 \text{ at } Y=-L/2 \quad \text{and} \quad C=C_2 \text{ at } Y=L/2 \tag{7}$$

The primitive boundary value problem is defined by Eqns. (1) to (7) which determine the velocity, temperature and nanoparticle volume fraction distribution. However, it is judicious to transform this system into non-dimensional form by introducing the following dimensionless parameters:

$$u=\frac{U}{U_0},\ \theta=\frac{T-T_0}{\Delta T},\ y=\frac{Y}{D},\ GR_T=\frac{g\,\beta_T\,\Delta T\,D^3}{\upsilon^2},\ \ Br=\frac{\mu U_0^2}{k\,\Delta T},\ \mathrm{Pr}=\frac{\upsilon}{\alpha},\ Le=\frac{\upsilon}{D_B},\ \mathrm{Re}=\frac{U_0\,D}{\upsilon},$$

$$\Lambda=\frac{GR_T}{\mathrm{Re}},\ Nb=\frac{(\rho C)_P\,D_B\,(C_2-C_1)}{(\rho C)_f\,\upsilon},\ \ Nt=\frac{(\rho C)_P\,D_T\,(T_2-T_1)}{(\rho C)_f\,\upsilon\,T_\infty},\ U_0=\frac{-AD^2}{48\mu},\ \phi=\frac{C-C_0}{\Delta C},\qquad (8)$$

$$Bi_1=\frac{h_1\,D_1}{k_1},\ Bi_2=\frac{h_2\,D_2}{k_2},\ R_T=\frac{T_2-T_1}{\Delta T},\ S=\frac{Bi_1\,Bi_2}{Bi_1\,Bi_2+2\,Bi_1+2\,Bi_2},\ Ec=\frac{\mu^2}{C_p\,\Delta T}$$

Here the hydraulic diameter is $D=2L$ and the reference velocity, reference temperature and reference nanoparticle volume fraction are written as:

$$U_0=-\frac{AD^2}{48\mu},\qquad T_0=\frac{T_1+T_2}{2}+S\left(\frac{1}{Bi_1}-\frac{1}{Bi_2}\right)\left[T_2-T_1\right],\qquad C_0=\frac{C_1+C_2}{2} \qquad (9)$$

Moreover, the temperature difference $\Delta T=T_2-T_1$, if $T_1<T_2$ and the concentration difference $\Delta C=C_2-C_1$ if $C_1<C_2$. Therefore, the reference temperature field difference $\Delta T=\frac{\nu^2}{C_p\,D^2}$, if $T_1=T_2$. As a consequence, the dimensionless parameter R_T can be either 0 or 1. More precisely, $R_T=1$ for *asymmetric* fluid temperatures at $T_1<T_2$ and $R_T=0$ for *symmetric* fluid temperatures at $T_1=T_2$. The dimensionless equations along with the boundary conditions are:

$$\frac{d^2u}{dy^2}=-48-\Lambda\,\theta \qquad (10)$$

$$\frac{d^2\theta}{dy^2}+Nb\ \mathrm{Pr}\ \frac{d\phi}{dy}\,\frac{d\theta}{dy}+Nt\ \mathrm{Pr}\left(\frac{d\theta}{dy}\right)^2+Ec\ \mathrm{Pr}\left(\frac{du}{dy}\right)^2=0 \qquad (11)$$

$$\frac{d^2\phi}{dy^2}+\frac{Nt}{Nb}\frac{d^2\theta}{dy^2}=0 \qquad (12)$$

$$u\left(-1/4\right)=u\left(1/4\right)=0 \qquad (13)$$

$$\left.\frac{d\theta}{dy}\right|_{y=-1/4}=Bi_1\left[\theta+\frac{R_T S}{2}\left(1+\frac{4}{Bi_1}\right)\right] \qquad (14)$$

$$\left.\frac{d\theta}{dy}\right|_{y=1/4} = Bi_2\left[-\theta + \frac{R_T S}{2}\left(1+\frac{4}{Bi_2}\right)\right] \tag{15}$$

$$\phi(-1/4) = -\frac{1}{2},\ \phi(1/4) = \frac{1}{2} \tag{16}$$

Clearly in Eqns. (14), (15) at the left duct wall a Biot number, Bi_1 is imposed and at the right duct wall a Biot number Bi_2 is prescribed. Biot number quantifies the relative importance of conduction and convection. The last term in the momentum Eqn. (10) denotes the thermal buoyancy force and the final term in the energy Eqn. (11) designated the viscous heating contribution.

3. Solutions of the boundary value problem

3a. *Regular perturbation solutions*

The transformed dimensionless boundary value problem defined by Eqns. (10)-(16) may be solved with a variety of methods. First a regular perturbation technique – see Rice and Do[70] is deployed to obtain analytical solutions wherein *Prandtl number* is selected as the perturbation parameter. The solutions for velocity, temperature and nanoparticle volume fraction (concentration) are therefore assumed in the following form:

$$u(y) = u_0(y) + (\mathrm{Pr})u_1(y) + (\mathrm{Pr})^2 u_2(y) + \ldots\ldots = \sum_{n=0}^{\infty} (\mathrm{Pr})^n u_n(y). \tag{17}$$

$$\theta(y) = \theta_0(y) + (\mathrm{Pr})\theta_1(y) + (\mathrm{Pr})^2 \theta_2(y) + \ldots\ldots = \sum_{n=0}^{\infty} (\mathrm{Pr})^n \theta_n(y). \tag{18}$$

$$\phi(y) = \phi_0(y) + (\mathrm{Pr})\phi_1(y) + (\mathrm{Pr})^2 \phi_2(y) + \ldots\ldots = \sum_{n=0}^{\infty} (\mathrm{Pr})^n \phi_n(y). \tag{19}$$

Substituting Eqns. (17) to (19) into Eqns. (10) to (16) and comparing the like powers of Eckert number, one obtains a sequence of boundary value problems.

In the *absence* of Prandtl number $(n = 0)$, Eqns. (10) to (16) take the form:

$$\frac{d^2 u_0}{dy^2} = 0 \tag{20}$$

$$\frac{d^2 \theta_0}{dy^2} = 0 \tag{21}$$

$$\frac{d^2\phi_0}{dy^2} = 0 \tag{22}$$

$$u_0(-1/4) = u_0(1/4) = 0 \tag{23}$$

$$\left.\frac{d\theta_0}{dy}\right|_{y=-1/4} = Bi_1\left[\theta_0 + \frac{R_T S}{2}\left(1+\frac{4}{Bi_1}\right)\right] \tag{24}$$

$$\left.\frac{d\theta_0}{dy}\right|_{y=1/4} = Bi_2\left[-\theta_0 + \frac{R_T S}{2}\left(1+\frac{4}{Bi_2}\right)\right] \tag{25}$$

$$\phi_0\left(-\frac{1}{4}\right) = -\frac{1}{2}, \quad \phi_0\left(\frac{1}{4}\right) = \frac{1}{2} \tag{26}$$

The exact solutions of Eqns. (20) to (22) can be obtained by *integrating twice* and the integration constants can be readily obtained via Eqns. (23) to (26) and are not presented for brevity.

In the *presence* of Prandtl number $(n>1)$, the boundary value problem emerges as:

$$\frac{d^2u_n}{dy^2} = \sum_{n=0}^{\infty} \Lambda\ \theta_n \tag{27}$$

$$\frac{d^2\theta_n}{dy^2} = \sum_{j=0}^{n-1} Nb\ \frac{d\phi_j}{dy}\frac{d\theta_{n-j-1}}{dy} + \sum_{j=0}^{n-1} Nt\ \frac{d\theta_j}{dy}\frac{d\theta_{n-j-1}}{dy} + \sum_{j=0}^{n-1} Ec\ \frac{du_j}{dy}\frac{du_{n-j-1}}{dy} \tag{28}$$

$$\frac{d^2\phi_n}{dy^2} = \frac{Nt}{Nb}\frac{d^2\theta_n}{dy^2} \tag{29}$$

$$u_n(-1/4) = u_n(1/4) = 0 \tag{30}$$

$$\left.\frac{d\theta_n}{dy}\right|_{y=-1/4} = Bi_1\left[\theta_n\right] \tag{31}$$

$$\left.\frac{d\theta_n}{dy}\right|_{y=1/4} = Bi_2\left[-\theta_n\right] \tag{32}$$

$$\phi_n\left(-\frac{1}{4}\right) = \phi_n\left(\frac{1}{4}\right) = 0 \tag{33}$$

The solutions of Eqns. (27) to (29) along with the conditions on the boundaries as provided in Eqns. (30)-(33) are solved by an iteration procedure. The solutions of zeroth order $(n=0)$ which are provided via Eqns. (20)-(23) are utilized to compute the solutions for the first order

$(n=1)$ and the process is continued for the required values of n. The solutions for $(n>1)$ are found using the symbolic software MATHEMATICA.

The skin friction, Nusselt and Sherwood number are key physical quantities defining the gradients of velocity, temperature and nanoparticle concentration at the duct walls. They are defined in non-dimensional form as follows:

$$\tau_1 = \left(\frac{du}{dy}\right)_{y=-\frac{1}{4}},\ \tau_2 = \left(\frac{du}{dy}\right)_{y=\frac{1}{4}} \tag{34}$$

$$Nu_1 = \left(\frac{1}{R_T\left[\theta(1/4)-\theta(-1/4)\right]+(1-R_T)}\right)\left[\frac{d\theta}{dy}\right]_{y=-1/4} \tag{35}$$

$$Nu_2 = \left(\frac{1}{R_T\left[\theta(1/4)-\theta(-1/4)\right]+(1-R_T)}\right)\left[\frac{d\theta}{dy}\right]_{y=1/4} \tag{36}$$

$$Sh_1 = \left(\frac{d\phi}{dy}\right)_{y=-\frac{1}{4}},\ Sh_2 = \left(\frac{d\phi}{dy}\right)_{y=\frac{1}{4}} \tag{37}$$

The average velocity $\bar{u}$ and the bulk temperature θ_b are given by:

$$\bar{u} = 2\int_{-1/4}^{1/4} u\ dy \tag{38}$$

$$\theta_b = \frac{2}{\bar{u}}\int_{-1/4}^{1/4} u\ \theta\ dy \tag{39}$$

3b. Numerical Solutions

The perturbation solutions obtained in the Section 3.1 are valid for values of Prandtl number less than one. However, this is a severe limitation for engineering applications, since it is known that the values of Prandtl number cannot be less than one if the working fluid is water (*Pr* = 7.56), n-butanol (*Pr* = 50), engine oil (*Pr* > 100), glycerin (*Pr* >1000) etc. In view of this the non-linear boundary value problem is therefore solved numerically using a Runge-Kutta shooting method for general values of all parameters. The solution values obtained numerically are verified where possible with the perturbation solutions obtained in section 3.1 and are also documented in **Tables 1, 2** for identical and differing Biot numbers at the duct walls.

Table 1. Comparison analysis when $Bi_1 = Bi_2 = 10$ (symmetric case)

y	Velocity					
	$Pr = 0$		$Pr = 0.01$		$Pr = 0.5$	
	Analytical	**Numerical**	**Analytical**	**Numerical**	**Analytical**	**Numerical**
-0.25	0.00000000	0.00000000	0.00000000	0.00000000	0.00000000	0.00000000
-0.15	0.95285714	0.95285714	0.95381995	0.95381571	1.00678237	1.00645116
-0.05	1.43642857	1.43642857	1.43789193	1.43788537	1.51827297	1.51783151
0.05	1.44357142	1.44357143	1.44503574	1.44502921	1.52535907	1.52498667
0.15	0.96714286	0.96714286	0.96810773	0.96810353	1.02096924	1.02077177
0.25	0.00000000	0.00000000	0.00000000	0.00000000	0.00000000	0.00000000
y	Temperature					
	$Pr = 0$		$Pr = 0.01$		$Pr = 0.5$	
	Analytical	**Numerical**	**Analytical**	**Numerical**	**Analytical**	**Numerical**
-0.25	-0.35714285	-0.35714286	-0.35104914	-0.35107134	-0.01290129	-0.01639941
-0.15	-0.21428571	-0.21428571	-0.20481394	-0.20485335	0.31864233	0.31407321
-0.05	-0.07142857	-0.07142857	-0.06140120	-0.06144869	0.49006895	0.48644152
0.05	0.07142857	1.44357143	0.08146984	0.08142289	0.63135011	0.62920684
0.15	0.21428571	0.21428571	0.22382221	0.22378434	0.74413759	0.74374912
0.25	0.35714285	0.35714286	0.36331946	0.36329874	0.69960297	0.70009068
y	Nanoparticle concentration					
	$Pr = 0$		$Pr = 0.01$		$Pr = 0.5$	
	Analytical	**Numerical**	**Analytical**	**Numerical**	**Analytical**	**Numerical**
-0.25	-0.50000000	-0.50000000	-0.50000000	-0.50000000	-0.50000000	-0.50000000
-0.15	-0.30000000	-0.30000000	-0.29957078	-0.30336129	-0.27810497	-0.48782784
-0.05	-0.10000000	-0.10000000	-0.09956478	-0.10390041	-0.07777136	-0.31704556
0.05	0.10000000	0.10000000	0.10043201	0.09610214	0.12208975	-0.11617065
0.15	0.30000000	0.30000000	0.30042135	0.29662336	0.32154342	0.11327558
0.25	0.50000000	0.50000000	0.50000000	0.49999996	0.50000000	0.49999999

Table 2. Comparison analysis when $Bi_1 = 1,\ Bi_2 = 10$ (asymmetric case)

y	Velocity					
	$Pr = 0$		$Pr = 0.01$		$Pr = 0.5$	
	Analytical	**Numerical**	**Analytical**	**Numerical**	**Analytical**	**Numerical**
-0.25	0.00000000	0.00000000	0.00000000	0.00000000	0.00000000	0.00000000
-0.15	0.95687499	0.95687500	0.95783782	0.95919346	1.01080022	1.11156275
-0.05	1.43843749	1.43843750	1.43990086	1.44176244	1.52028191	1.66028122
0.05	1.44156250	1.44156250	1.44302681	1.44471718	1.52335014	1.65205614
0.15	0.96312499	0.96312500	0.96408987	0.96510300	1.01695138	1.09509587
0.25	0.00000000	0.00000000	0.00000000	0.00000000	0.00000000	0.00000000
y	Temperature					
	$Pr = 0$		$Pr = 0.01$		$Pr = 0.5$	
	Analytical	**Numerical**	**Analytical**	**Numerical**	**Analytical**	**Numerical**
-0.25	-0.15625000	-0.15625000	-0.15015628	-0.12970162	0.18799156	1.61615507
-0.15	-0.09375000	-0.09375000	-0.08427823	-0.06728545	0.43917804	1.67174283
-0.05	-0.03124999	-0.03125000	-0.02122263	-0.00768228	0.53024753	1.54099596
0.05	0.03125000	0.03125000	0.04129127	0.05141043	0.59117155	1.37700776
0.15	0.09375000	0.09375000	0.10328650	0.11000216	0.62360187	1.17781202
0.25	0.15625000	0.15625000	0.16242661	0.16576674	0.49871011	0.78988839
y	Nanoparticle concentration					
	$Pr = 0$		$Pr = 0.01$		$Pr = 0.5$	
	Analytical	**Numerical**	**Analytical**	**Numerical**	**Analytical**	**Numerical**
-0.25	-0.50000000	-0.50000000	-0.50000000	-0.50000000	-0.50000000	-0.50000000
-0.15	-0.30000000	-0.30000000	-0.29957078	-0.30330638	-0.27810497	-0.51617480
-0.05	-0.10000000	-0.10000000	-0.09956478	-0.10380754	-0.07777136	-0.34707423
0.05	0.10000000	0.10000000	0.10043201	0.09619361	0.12208976	-0.14716172
0.15	0.30000000	0.30000000	0.30042134	0.29668751	0.32154342	0.08506396
0.25	0.50000000	0.50000000	0.50000000	0.49999996	0.50000000	0.50000003

Table 3 Validation with Zanchini[45]

y	$Bi_1 = Bi_2 = 10$ $u = u_0 + Pr\ u_1 + Pr^2 u_2 + Pr^3 u_3 + Pr^4 u_4 + Pr^5 u_5 + Pr^6 u_6 + Pr^7 u_7$			
	Velocity		**Temperature**	
	Zanchini[57]	Present $Nt = Nb = 0$	Zanchini[57]	Present $Nt = Nb = 0$
-0.25	0.00000000	0.00000000	-0.35703534	-0.35708205
-0.15	0.81752467	0.81715247	-0.21410689	-0.21419119
-0.05	1.36916041	1.36858603	-0.07122816	-0.07132849
0.05	1.51202552	1.51144318	0.07163487	0.07152879
0.15	1.10325604	1.10286677	0.21449135	0.21438090
0.25	0.00000000	0.00000000	0.35728439	0.35720451

Tables 1 to 3 show the comparison of solutions for u, θ and ϕ which are estimated by the regular perturbation method described in section 3.1, considering seven terms of the series and also those obtained numerically by the Runge-Kutta shooting method for the *symmetric* heating case, $Bi_1 = Bi_2 = 10$ (**Table 1**) and the *asymmetric* heating case, $Bi_1 = 1$, $Bi_2 = 10$ (**Table 2**) for variation in Prandtl number, Pr. The parameter values are fixed are $Nt = Nb = 0.1, Ec = 0.01, \Lambda = 5, R_T = 1$ in **Tables 1 and 2**. These physically imply weak thermophoresis (Nt =0.1), large nanoparticle diameters (Nb = 0.1), weak viscous heating (Ec = 0.01), strong thermal buoyancy (Λ = 5) and a *asymmetric* fluid temperature case between the duct walls (R_T= 1). These represent realistic scenarios in buoyancy-driven nanofluid duct transport as noted in Das *et al.*[71] and Gebhart *et al.*[72] and also concur with data specification in other recent simulations in nanofluid mechanics based on the Buongiorno formulation[33-35, 45]. In the absence of Prandtl number the analytical and numerical values *are equal* for all values of Bi (**Tables 1 and 2**). The perturbation and numerical shooting values match for up to four decimal places for identical Bi and up to two decimal places for dissimilar Bi when Pr = 0.01. The analytical and numerical values concur up to two decimal places $(Bi_1 = Bi_2 = 10)$ although they

deviate considerably $(Bi_1 = 1,\ Bi_2 = 10)$ when Pr = 0.5. The solutions are also validated against Zanchini[57] in the absence of nanoparticles as presented in **Table 3** and found to be in excellent agreement. Overall confidence in the perturbation and shooting numerical solutions is therefore justifiably high. In the next section computations based on the shooting method are visualized in graphs and Tables.

4. Results and discussion

The transport characteristics for the nanofluid flow in a vertical duct have been computed via Runge-Kutta quadrature solutions of Eqns. (10) to (16) and the results are depicted graphically in **Figs. 2- 6**. The impact of thermal Grashof number Λ, Prandtl number Pr, Eckert number Ec, thermophoresis parameter Nt and Brownian dynamics parameter Nb for identical and dissimilar wall temperatures and Biot numbers is examined in detail in these figures. **Tables 4-6** furthermore provide results for skin friction values (dimensionless wall shear stress), Nusselt numbers at both duct walls (dimensionless wall heat transfer rate), mean velocity, bulk temperature and Sherwood numbers at the two duct boundaries (dimensionless wall nanoparticle mass transfer rate) with selected thermophysical parameters to furnish additional insights into the convective flow transport in the duct.

Figures 2a to 2d shows the response of Λ on the velocity field, temperature field and nanoparticle volume fraction ϕ for equal Biot numbers. An increment in Λ, produces an amplification in thermal buoyancy force (i.e. $\Lambda\theta$ in the momentum eqn. (10)). This inflates both velocity (u) and temperature (θ) (Figs. 2a, b) whereas nanoparticle concentration (ϕ) (Fig. 2c) is declined for all values of transverse coordinate, y. A symmetric velocity distribution is computed between the duct walls as per the symmetric heating case. For $\Lambda = 0$ *the forced convection case is retrieved, and the momentum and energy equations are decoupled.* Thermal buoyancy therefore clearly energizes the regime but *inhibits* nanoparticle diffusion in the duct.

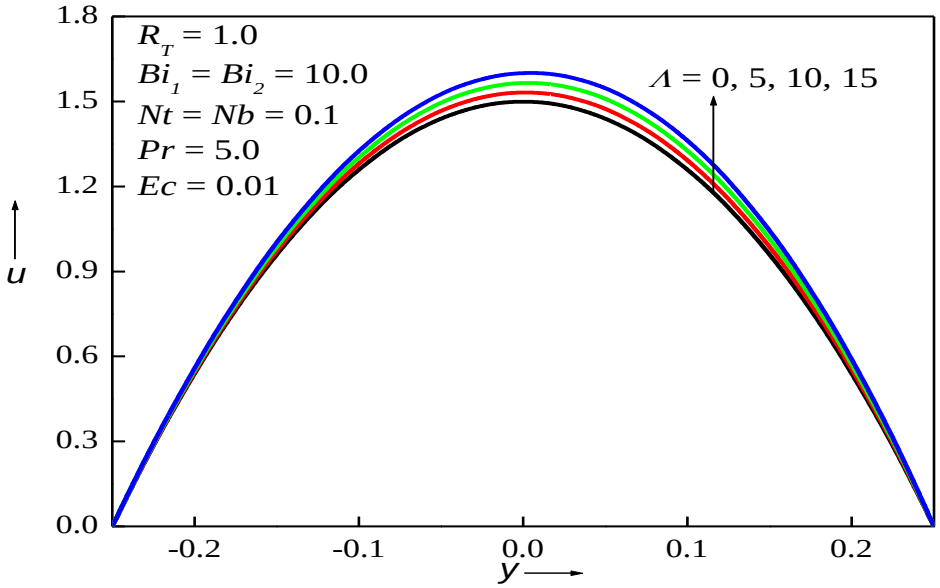

Figure 2a. Effects of Λ on velocity profile for equal Biot number

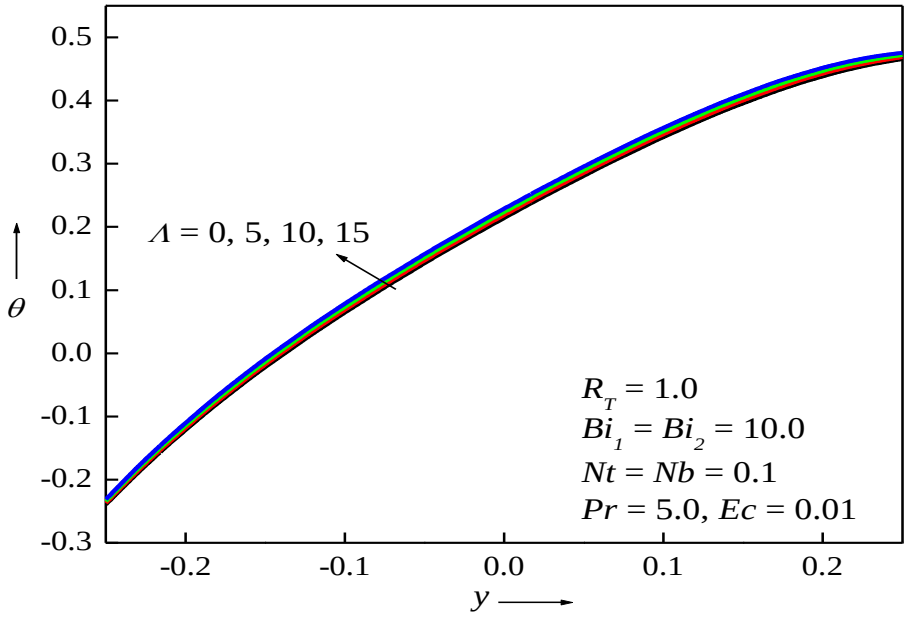

Figure 2b. Effects of Λ on temperature with equal Biot numbers

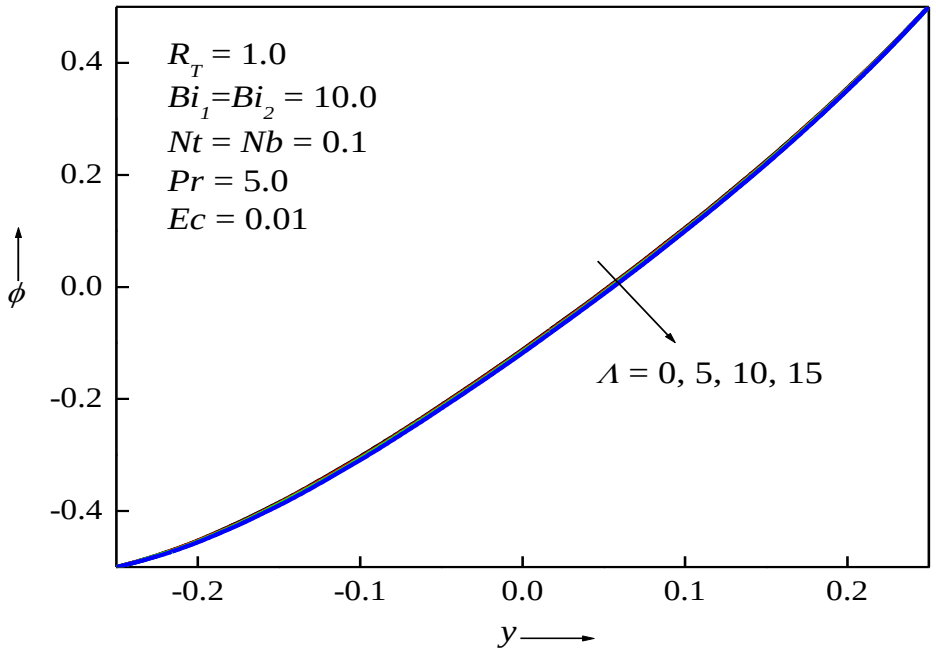

Figure 2c. Effects of Λ on nanoparticle volume fraction field with equal Biot numbers

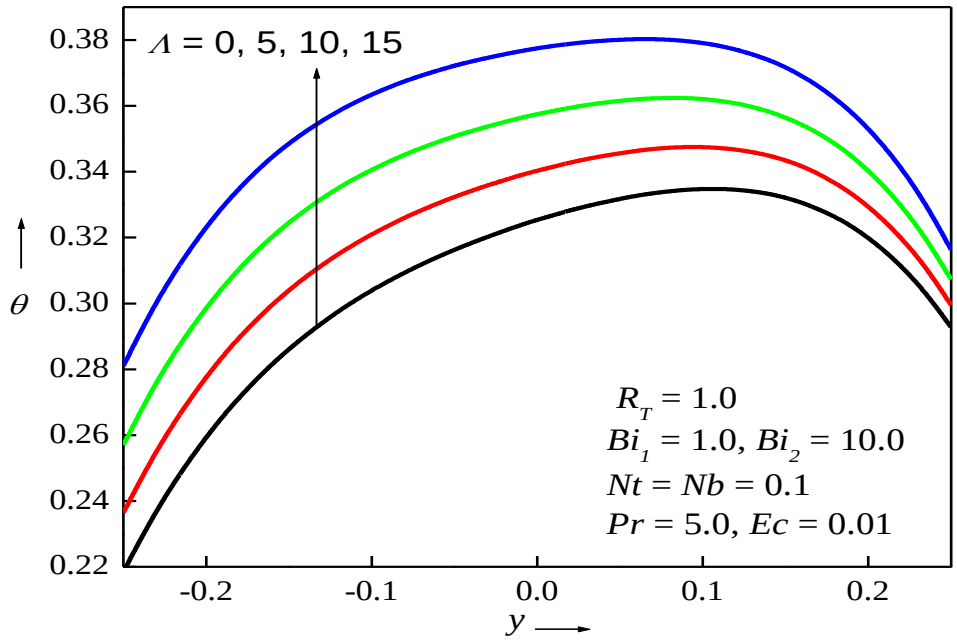

Figure 2d. Effects of Λ on temperature field with unequal Biot numbers

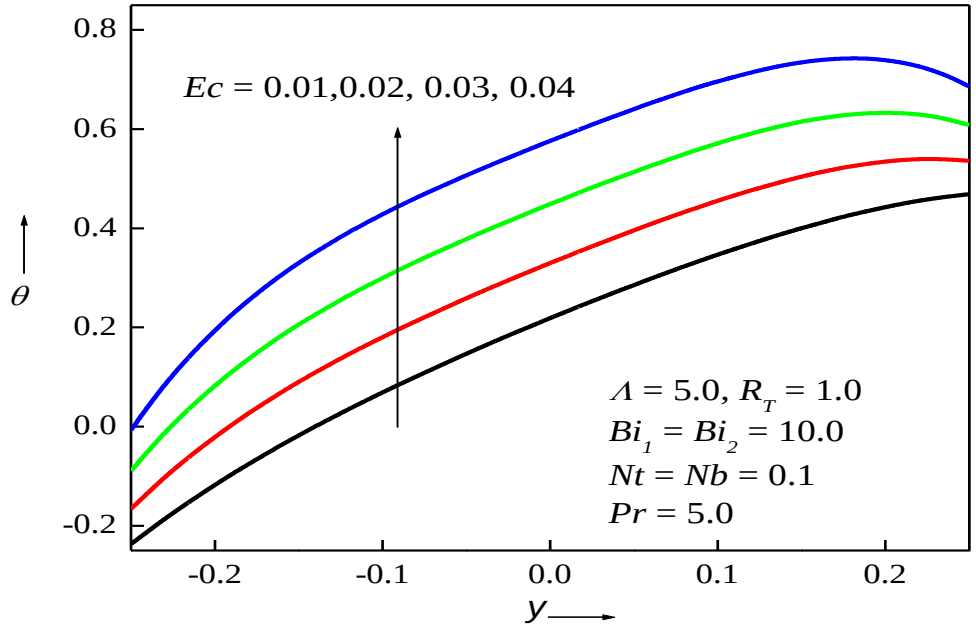

Figure 3a. Effects of *Ec* on temperature field with equal Biot number

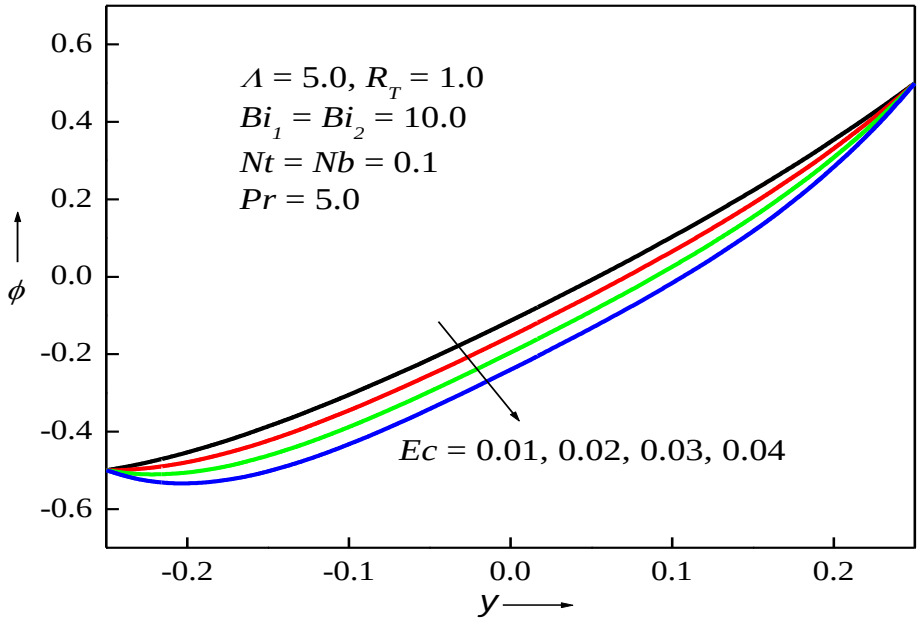

Figure 3b. Effects of *Ec* on nanoparticle volume fraction field with equal Biot numbers

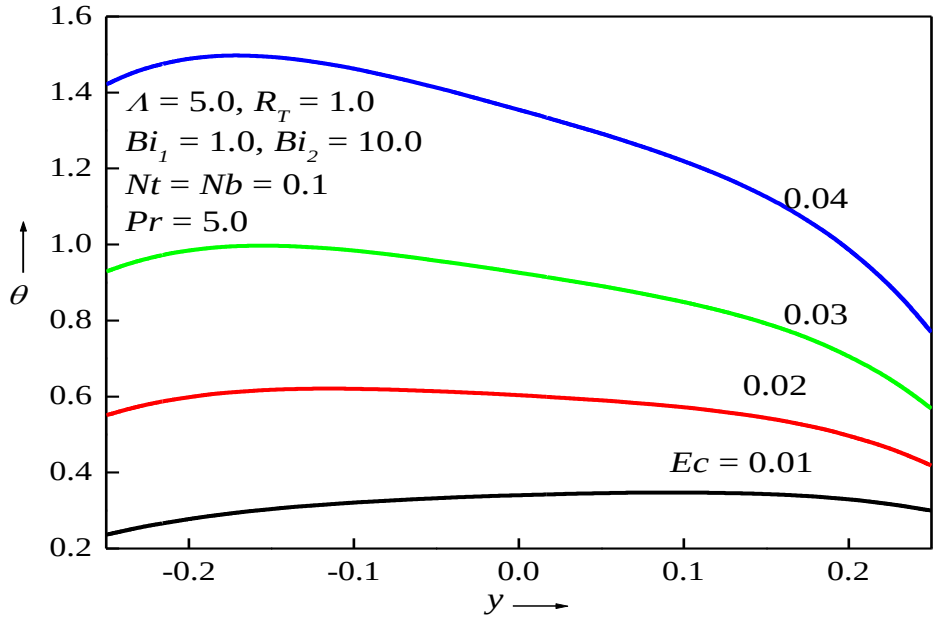

Figure 3c. Effects of *Ec* on temperature filed with unequal Biot numbers

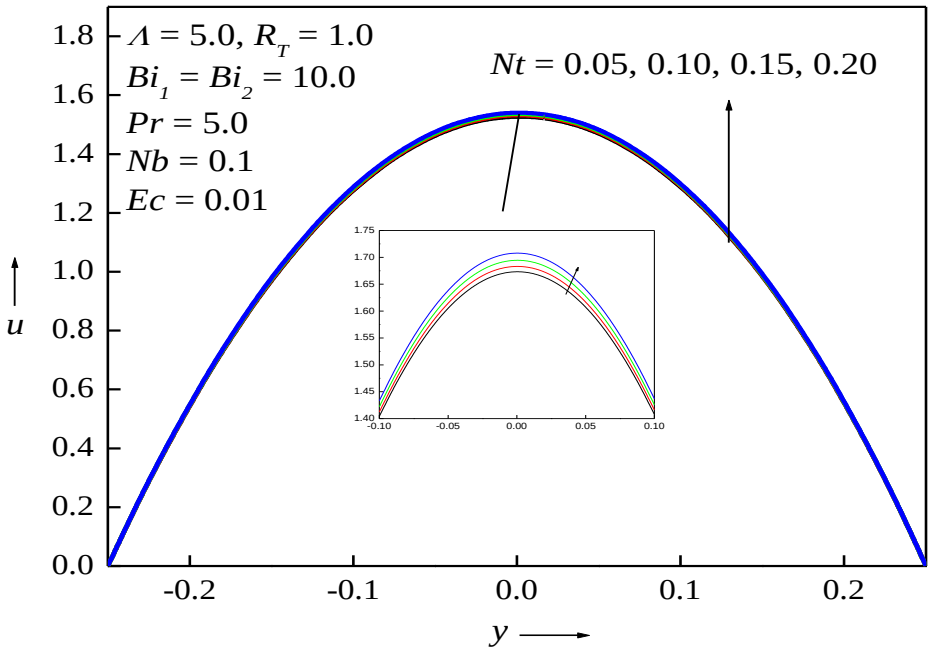

Figure 4a. Effects of *Nt* on velocity field with equal Biot numbers

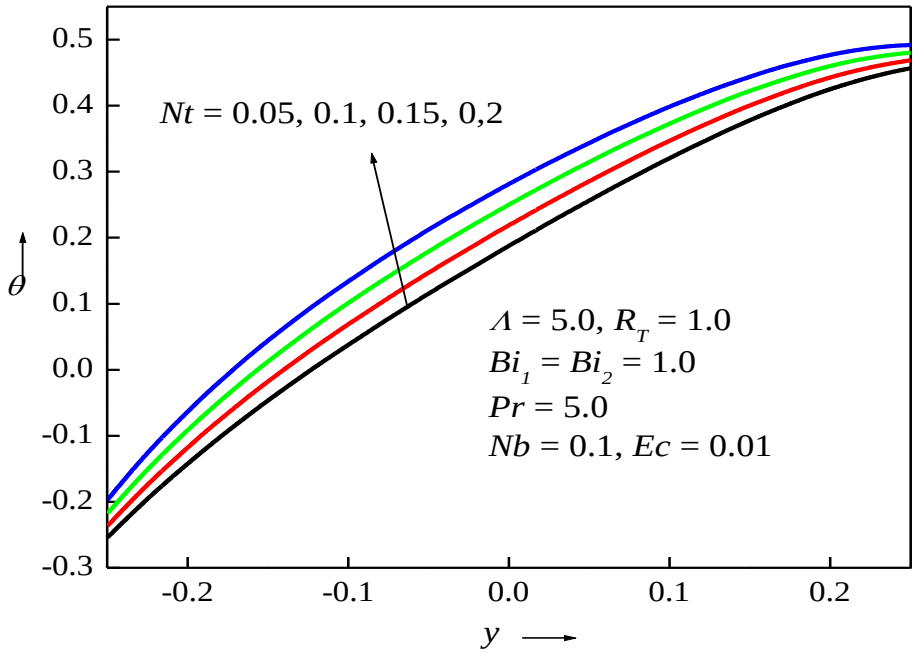

Figure 4b. Effects of *Nt* on temperature field with equal Biot numbers

Table 4. Nusselt numbers at the duct walls, mean velocity and bulk temperature

$Bi_1 = Bi_2 = 10$					$Bi_1 = 1.0, Bi_2 = 10$			
	Nu_1	Nu_2	$\bar{u}$	θ_b	Nu_1	Nu_2	$\bar{u}$	θ_b
Λ								
0	6.28571	-2.28571	1.00000	0.48367	-3.62459	7.62460	1.00000	1.07019
5	6.21932	-2.30216	1.05039	0.48459	-3.64736	7.69626	1.11129	1.06884
10	6.15447	-2.31918	1.10080	0.48555	-3.67039	7.76901	1.22221	1.06742
15	6.09115	-2.33676	1.15128	0.48655	-3.69369	7.84286	1.33277	1.06597
Ec								
0.2	3.74505	0.22170	1.02092	0.20171	-39.9316	44.2910	1.04502	0.43224
0.4	5.39652	-1.46287	1.04057	0.39029	-4.60856	8.66568	1.08920	0.85655
0.6	7.04018	-3.13947	1.06021	0.57888	-3.14687	7.19149	1.13338	1.28120
0.8	8.67609	-4.80816	1.07985	0.76748	-2.63239	6.67260	1.17755	1.70614
Nb								

0.5	6.41814	-2.50098	1.05336	0.51316	-3.58052	7.62786	1.11387	1.09367
1.0	6.66666	-2.74949	1.05708	0.54888	-3.50275	7.54827	1.11712	1.12472
1.5	6.91518	-2.99802	1.06080	0.58459	-3.43073	7.47457	1.12033	1.15576
2.0	7.16369	-3.24654	1.06452	0.62032	-3.36385	7.40612	1.12356	1.18681
Nt								
0.5	6.36133	-2.44417	1.05251	0.50499	-3.62600	7.67441	1.11210	1.07656
1.0	6.53885	-2.62169	1.05517	0.53051	-3.59991	7.64775	1.11311	1.08636
1.5	6.71636	-2.79920	1.05783	0.55602	-3.57447	7.62167	1.11412	1.09599
2.0	6.89388	-2.97672	1.06049	0.58154	-3.54966	7.59627	1.11513	1.10569

Table 5. Skin friction at the duct walls

	$Bi_1 = Bi_2 = 10$		$Bi_1 = 1.0, Bi_2 = 10$	
	τ_1	τ_2	τ_1	τ_2
Λ				
0	12.00000	-12.00000	12.00000	-12.00000
5	12.42669	-12.72650	13.41912	-13.19741
10	12.85145	-13.45555	14. 83175	-14.39242
15	13.27469	-14.18747	16.23807	-15.58516
Ec				
0.2	12.08980	-12.38830	12.53515	-12.52315
0.4	12.31437	-12.61377	13.12446	-12.97265
0.6	12.53895	-12.83923	13.71376	-13.42216
0.8	12.76353	-13.06469	14.30307	-13.87166
Nb				
0.5	12.45941	-12.75924	13.45248	-13.22345
1.0	12.50032	-12.80016	13.49418	-13.25600
1.5	12.54125	-12.84108	13.53589	-13.28855
2.0	12.58217	-12.88201	13.57760	-13.32110
Nt				

0.5	12.45000	-12.74988	13.42954	-13.20554
1.0	12.47928	-12.77911	13.44257	-13.21572
1.5	12.50851	-12.80834	13.45561	-13.22589
2.0	12.53774	-12.83757	13.46864	-13.23606

Table 6. Sherwood numbers at the duct walls

$Bi_1 = Bi_2 = 10$			$Bi_1 = 1.0, Bi_2 = 10$	
	Sh_1	Sh_2	Sh_1	Sh_2
Λ				
0	-1.08736618	5.03454007	-0.99475944	4.98130461
5	-1.40624107	5.41013820	-2.00147219	5.91705800
10	-1.84693384	5.91476734	-5.82171186	9.40026140
15	-2.51343205	6.65587803	-0.74800028	9.45692636
Ec				
0.2	0.68692558	3.31456569	0.67275847	3.31222724
0.4	-0.67620980	4.67958332	-0.97966397	4.92670672
0.6	-2.17281857	6.17691432	-3.21943416	7.09209462
0.8	-3.83149355	7.83483138	-6.72699001	10.46155367
Nb				
0.5	1.27245427	2.69887885	1.20836910	2.74070990
1.0	1.60626747	2.35894131	1.61061527	2.34034039
1.5	1.71677939	2.24486494	1.74545474	2.20440879
2.0	1.77146532	2.18725323	1.81344648	2.13457734
Nt				
0.2	-4.90142387	8.85639533	-6.07302842	9.97803437
0.4	-12.1634587	15.8505076	-14.4380157	18.5849291
0.6	-19.7962755	22.9690351	-23.1198214	27.9433111
0.8	-27.8109358	30.1992474	-32.1465766	38.2078054

The forced convection case (Λ = 0) therefore achieves maximum nanoparticle concentration magnitudes whereas the strong natural convection case (Λ = 15) achieves maximum flow acceleration and peak temperature in the duct regime. A monotonic (*concave*) ascent in temperatures from the left duct wall to the right duct wall is computed at all values of the thermal buoyancy parameter whereas a *convex monotonic ascent* is observed for nanoparticle concentration when Biot numbers are equal at both duct walls. Fig. 2d demonstrates that for the asymmetric case (unequal Biot numbers) a strong modification in temperature distributions is computed which deviates significantly from the symmetric Biot number case (Fig. 2b). The profiles become increasingly curved and more prominently warped towards the left duct wall. Profiles near the right duct wall are also more constricted indicating that in the proximity of the right wall there is less modification in temperatures with increment in thermal buoyancy effect. As anticipated, the unequal Biot numbers induce a non-symmetrical topology in the temperature profiles and the peak is also nearer the right wall. As with the symmetric Biot number case, the forced convection scenario (Λ = 0) minimizes temperature magnitudes whereas the extreme natural (free) convection scenario (Λ = 15) produces peak temperatures. The sensitivity of the temperature field to both buoyancy and wall thermal boundary conditions is therefore clearly captured.

The influence of Eckert numbers Ec on the temperature field and nanoparticle volume fraction field is presented in **Figs 3a-3c**. The Eckert number Ec is the parameter which quantifies the ratio of the heat dissipation via internal friction to the enthalpy difference (or the dynamic temperature to the temperature) driving force in convective transport. Therefore this number quantifies the relative effectiveness of heat dissipation transport by diffusion on θ and ϕ. These figures reveal that as the Eckert number increases, temperature enhances but ϕ is diminished for similar and distinct Biot numbers. Clearly increasing viscous heating energizes the duct flow due to conversion of mechanical energy into heat. However, this boost in temperature and thermal diffusion has a counter-productive impact on nanoparticle species diffusion (the concentration conservation equation does not feature a dissipation term, and therefore the effect is indirect). The influence of Ec on the momentum is to decelerate flow due to dissipation of mechanical energy at all values of Bi which is a similar outcome to that seen in Figs. 2a and 2d and hence not exhibited. It is also interesting to note that for the symmetric

heating case (equal Biot numbers) the maximum temperature is computed for *Ec* = 0.04 closer to the right duct wall. However, for the asymmetric case (unequal Biot numbers) the peak temperature again for *Ec* = 0.04 is displaced closer to the left duct wall.

Figures 4a-4b and supplementary Figs. 4c and 4d shows the evolution in u, θ and ϕ across the duct with thermophoresis parameter, *Nt*, for distinct and identical values of Biot numbers. The impact of *Nt* on the velocity field is relatively minor (it induces a weak acceleration, notably in the core zone of the duct) whereas it significantly modifies temperatures and results in an intensification in temperature magnitudes for all values of Biot numbers. *Nt* is one of two nanoscale parameters featured in the Buongiorno model which arises in two terms in the model- viz the second degree temperature term, $+Nt\,\mathrm{Pr}\left(\frac{d\theta}{dy}\right)^2$ in the energy Eqn. (11) and the coupling term, $\frac{Nt}{Nb}\frac{d^2\theta}{dy^2}$ in the nanoparticle (volume fraction) concentration Eqn. (12). *Nt* is associated with the thermophoretic body forces generated by temperature gradient which transports nanofluid molecules from a region of high temperature (i.e. near the surface- specifically the duct walls) to a region of low temperature (i.e. far away from the surface, viz core region of the duct). This enhances temperatures in the enture duct space. Conversely the nanoparticle concentration field is dwindled for larger values of *Nt* (Supplementary Fig. 4c). At very low *Nt* (= 0.05) the concentration distribution is approximately linear and ascends from the left wall to the right wall. However, the profiles become increasingly parabolic with increment in thermophoresis parameter (*Nt* =0.1, 0.15, 0.2) despite the suppression in concentration (nanoparticle volume fraction) magnitudes. As noted earlier, the unequal Biot number case (asymmetric heating) produces a shift in the peak temperature further away from the right duct wall, whereas the peak is much closer to the right wall for the equal Biot number scenario (symmetric heating). Furthermore, the profiles are distinctly inverted parabolas for the asymmetric case (Supplementary Fig. 4d) whereas they exhibit a distinctly monotonic nature for the symmetric heating case (Fig. 4b). However, the thermophoresis body force exerts the same overall effect for both heating cases- it enhances temperature across the duct.

The influence of the second nanoscale parameter, Brownian motion parameter, *Nb* on u and θ is similar to the impact computed with *Nt* and hence is not presented. The outcome of

Nb on nanoparticle volume fraction ϕ is however visualized in **Supplementary Fig 5**, and clearly produces An elevation in ϕ i.e. encourages nanoparticle diffusion for equivalent Bi (the trend is similar for divergent Bi and is therefore not displayed). Large values of this parameter correspond to smaller spherical nanoparticles and vice versa for lower *Nb* values (larger diameter nanoparticles), as elaborated in Buongiorno[35] , Bég *et al.*[73] and Thumma *et al.*[75]. Larger *Nb* values clearly produce smaller nanoparticles which mobilzes improved diffusion in the duct regime. The parameter, *Nb*, arises again in two terms in the model, namely the mixed derivative term, $Nb\,\mathrm{Pr}\frac{d\phi}{dy}\frac{d\theta}{dy}$ in the energy Eqn. (11) and the coupling term, $\frac{Nt}{Nb}\frac{d^2\theta}{dy^2}$ in the nanoparticle (volume fraction) concentration Eqn. (12). Interms of ballistic collisions of nanoparticles, an increasing value of *Nb* accelerates the flow and in turn influences kinetic energy $\left(\frac{1}{2}mv^2=\frac{3}{2}K_B T\right)$ where K_B is Boltzmann constant which influences the temperature distribution (Brownian motion is associated with balllistic collisons of nanoparticles). This assists in nanoparticle diffusion in the regime, as noted by Das *et al.*[59].

Figures 2 to 4b and supplementary Figs. 4c to 5 correspond to $R_T = 1$. For equal wall temperatures, the action of thermal buoyancy parameter, $\Lambda=Gr_T/Re$ (as defined in Eqn. (8), on u, θ and ϕ is depicted in **Supplementary Figs. 6a to 6d.** The momentum, energy and concentration fields are all consistently escalated by augmenting Λ for all values of Bi. In other words, the duct flow is accelerated and both temperature and nanoparticle concentration (volume fraction) are accentuated with stronger thermal buoyancy effect (Λ *= 5, 10 i.e. natural convection)* whereas the reverse trend is computed for forced convection (Λ *=0* i.e. vanishing thermal buoyancy effect). However, a weaker increase in nanoparticle concentration is produced (Supplementary Fig. 6c) compared with the boost in velocity and temperature magnitudes (Supplementary Figs. 6a, b). From all the figures one can conclude that the performance of Bi is more prominent at the cold duct wall for unequal Biot numbers when compared with equal Biot numbers. The impact of Prandtl number is omitted since the profiles are qualitatively similar to the influence of the Eckert number.

The values of Nu (Nusselt number), $\bar{u}$ (mean velocity) and θ_b (bulk temperature) are illustrated in **Table 4**. The Nusselt values are lowered with Λ and are enhanced with Ec, Nb, Nt at the left wall whereas Nusselt numbers are increased in magnitude at the right wall by boosting Λ, Ec, Nb, Nt for identical Biot numbers (symmetric case). For distinct Biot numbers (asymmetric case), Nu at the left plate increases in magnitude with increment in thermal buoyancy parameter, Λ and is lowered in magnitude with greater values of Ec, Nb, Nt. The Nusselt values at the right plate are intensified with Λ whereas they are suppressed with magnification in Ec, Nb, Nt when $Bi_1 = 1,\ Bi_2 = 10$. The mean velocity exhibits an upsurge with increasing values of Λ, Ec, Nb, Nt for all values of Bi. The bulk temperature is boosted by raising Λ, Ec, Nb, Nt for *equal Biot numbers* whereas it is depleted with increment in Λ and expanded with augmenting Ec, Nb, Nt for *unequal* Biot numbers. The skin friction at the cold wall (left) is intensified with Λ, Ec, Nb, Nt and declined at the hot wall (right) with Λ, Ec, Nb, Nt for all values of Bi as shown in **Table-5**. The values of Sh (Sherwood number) at both the left and right duct walls are depicted in **Table-6**. Sh at the cold wall is reduced i.e. nanoparticle mass transfer rate to the wall is depressed by increasing Λ, Ec, Nt whereas it is elevated with a rise in Nb for all values of Bi. At the hot wall Sh is markedly scaled up with an increase in Λ, Ec, Nb, Nt for all values of Bi.

5. Conclusions

A comprehensive mathematical model for dissipative nanofluid buoyancy-driven flow in a thermal duct with Fourier-type boundary conditions has been developed, motivated by applications in thermal process engineering. The two-component Bungiorno nanoscale model has been deployed. The duct left wall temperature is kept lower than that of the right wall. The non-dimensional coupled conservation equations for momentum, heat and nanoparticle concentration have been solved with appropriate boundary conditions using a regular perturbation method for Prandtl number, Pr <1. Numerical solutions with an efficient Runge-Kutta shooting method, have also been presented at all values of the control parameters for $(Pr \leq 1, Pr > 1)$. The solutions obtained by the shooting method and perturbation method

match exactly for $Pr = 0$ whereas they deviate as Pr increases. For regular Newtonian viscous fluid the results agree very closely with Zanchini[45]. The present simulations have shown that:

1. With increasing thermal Grashof number, temperature and velocity are accentuated through the duct whereas nanoparticle concentration magnitudes are depleted, for both equal and unequal Biot numbers.
2. With increasing Eckert number, temperature is strongly elevated in the duct and nanoparticle concentration magnitudes are reduced, again for both equal and unequal Biot numbers.
3. The magnitude of intensification of the temperatures at the hot wall is predominant for unequal Biot numbers in comparison with identical duct wall Biot numbers.
4. Increment in thermophoresis and Brownian motion parameters boosts both velocity and temperature magnitudes for all values of Biot number prescribed at the duct walls i.e. both symmetric and asymmetric cases. However, elevation in thermophoresis parameter suppresses the nanoparticle concentration field whereas the Brownian motion effect enhances the nanoparticle concentration magnitudes across the duct span.
5. Nusselt number values are lowered with increasing thermal buoyancy parameter whereas they are magnified with Eckert number, Brownian motion parameter and thermophoresis parameter at the cold duct wall (left).
6. Nusselt number values at the hot duct wall, are enhanced with an increment in thermal buoyancy parameter, Eckert number, Brownian motion parameter and thermophoresis parameter for equal Biot numbers. The opposite trend is computed for different Biot numbers.
7. Strong natural convection generally accelerates the flow and elevates temperatures and nanoparticle concentrations compared with forced convection (vanishing thermal buoyancy effect).
8. For any given values of Biot numbers, the mean velocity and bulk temperature are boosted with increment in thermal buoyancy parameter, Eckert number, Brownian motion parameter and thermophoresis parameter.

9. The skin friction at the cold wall (left) is intensified with larger values of thermal buoyancy parameter, Eckert number, Brownian motion parameter and thermophoresis parameter whereas it is suppressed at the hot wall (right) for all values of Bi.
10. Sherwood numbers (i.e. dimensionless nanoparticle mass transfer rate to the duct walls) are diminished at the cold left wall with increasing thermal buoyancy parameter, Eckert number and thermophoresis parameter whereas they are amplified with stronger Brownian motion parameter Nb. At the hot wall the Sherwood numbers are however magnified with increment in all these parameters.

The present study has provided some deeper insight into thermofluid characteristics of nanofluids as deployed in duct systems. Future investigations may generalize the analysis to consider multiple (*hybrid*) nanoparticles (triple diffusion) as opposed to *unitary* nanofluids[75], porous media and more complex duct wall features (e.g. wavy walls)[76, 77] and efforts in this direction are currently underway.

REFERENCES:

1. Eastman JA, Choi SUS, Li S, Yu W and Thompson LJ. Anomalously increased effective thermal conductivities of ethylene glycol-based nanofluids containing copper nanoparticles. *Applied Physics Letters* 2001: 78: 718-720.

2. Nageswara *et al.* T. Enhanced thermal properties of silica nanoparticles and chitosan bio-based intumescent flame-retardant Polyurethane coatings. *Materials Today: Proceedings* 2020; 27: 369-375.

3. Umavathi JC, Bég OA, Gorla RSR and Vasu B. Perturbation and MAPLE quadrature computation of thermo-solutal dissipative reactive convective flow in a geothermal duct with Robin boundary conditions, *TFRE 2020: International Conference on Recent Trends in Developments of Thermo-fluids and Renewable Energy,* NIT Arunachal Pradesh, Yupia, India, 24-26 June 2020.

4. Xiu *et al.* TF. Al-nanoparticle-containing nanofluid fuel: synthesis, stability, properties, and propulsion performance. *Ind. Eng. Chem. Res.* 2016; 55: 2738–2745.

5. Umavathi JC and Bég OA. Modelling the onset of thermosolutal convective instability in a non-Newtonian nanofluid-saturated porous medium layer. *Chinese J. Physics* 2020; 68: 147–167.

6. Zhang Y. Experimental study on the effect of nanoparticle concentration on the lubricating property of nanofluids for MQL grinding of Ni-based alloy. *Journal of Materials Processing Technology*. 2016; 232: 100-115.

7. Umavathi JC, Ojjela O and Vajravelu K. Numerical analysis of natural convective flow and heat transfer of nanofluids in a vertical rectangular duct using Darcy-Forchheimer-Brinkman model. *Int. J. Thermal Sci*. 2017; 111: 511-524.

8. Anoop *et al.* K. Thermal evaluation of nanofluids in heat exchangers. *International Communications in Heat and Mass Transfer*. 2013; 49: 5-9.

9. Tripathi J, Vasu B, Bég OA. Computational simulations of hybrid mediated nano-hemodynamics (Ag-Au/blood) through an irregular symmetric stenosis. *Computers in Biology and Medicine*. 2021; 130. 104213 doi.org/10.1016/j.compbiomed.2021.104213

10. Hu Z., Siddeequah MA, Ghulam R, Paul WJG, Dongsheng W. Nanoparticle-assisted water-flooding in Berea sandstones. Energy Fuels. 2016; 30: 2791–2804.

11. Kuharat S, Bég OA, Bég TA, Kadir A, Leonard HJ, Walid SJ. CFD simulation of diamond and zinc smart nanoparticles performance in a water-based trapezium direct absorber solar collector (DASC), *Materials of the Future: Smart Applications in Science and Engineering 2021 E-conference, Center for Advanced Materials (CAM) and Biomedical Research Center (BRC).* Qatar University, Qatar , 29-31 March 2021.

12. Dickinson E. Use of nanoparticles and microparticles in the formation and stabilization of food emulsions. *Trends Food Sci. Technol*. 2012; 24: 4–12.

13. Bég OA. Nonlinear multi-physical laminar nanofluid bioconvection flows: Models and computation. *A. Sohail, Z. Li (Eds.): Computational Approaches in Biomedical Nano-Engineering.* Wiley, Chapter 5, 2018; 113-145.

14. Masuda H, Ebata A, Teramee K, Hishimura N. Alteration of thermal conductivity and viscosity of liquid by dispersing ultra-fine particles. *Netsu Bussei (Japan).* 1993; 4: 227-233.

15. Lee S, Choi S U S, Li S, Eastman JA. Measuring thermal conductivity of fluids containing oxide nanoparticles. *ASME J. Heat Transfer*. 1999; 121: 280-289.

16. Xuan Y, Roctzel W. Conceptions for heat transfer correlations of nanofluids. *Int. J. Heat Mass Transfer*. 2000; 43: 3701-3707.

17. Buongiorno J. A benchmark study on the thermal conductivity of nanofluids. *J. Applied Physics*. 2009; 106: 094312-1-094312-14.

18. Lee S, Choi SUS. Application of metallic nanoparticle suspensions in advanced cooling systems. *Int. Mechanical Engineering Congress and Exhibition.* Atlanta, U. S. A. 1996; 1-12.

19. Jang SP, Choi SUS. Cooling performance of a microchannel heat sink with nanofluids. *Applied Thermal Engineering*. 2006; 26: 2457-2463.

20. Heris SZ, Esfahany MN and Etemad SG. Experimental investigation of convective heat transfer of Al_2O_3 / water nanofluid in a circular tube. *Int. J. Heat Fluid Flow*. 2007; 28: 203-210.

21. Pak BC, Cho Y. Hydrodynamic and heat transfer study of dispersed fluids with submicron metallic oxide particles. *Exp. Heat Transfer*. 1998; 11: 151-170.

22. Chein R, Chuang J. Experimental microchannel heat sink performance studies using nanofluids. *Int. J. Thermal Sciences*. 2007; 46: 57-66.

23. Lee J, Mudawar I. Assessment of the effectiveness of nanofluids for single phase and two-phase heat transfer in microchannels. *Int. J. Heat Mass Transfer*. 2007; 50: 452-463.

24. Dring Y, Chen H, Wang L, Yang CY, He Y, Yang W, Lee WP, Zhang L, Huo R. Heat transfer intensification using nanofluids. *KONA*. 2007; 25: 23-38.

25. Wang XQ, Mujumdar AS. Heat transfer characteristics of nanofluids: a review. *Int. J. Thermal Sciences*. 2007; 46: 1-19.

26. Hu Ge-JiLe , Nehad AS, Mahrous YM, Pooja S, Raju CSK, Mamatha SU. Radiated magnetic flow in a suspension of ferrous nanoparticles over a cone with Brownian motion and thermophoresis. *Case Studies in Thermal Engineering*. 2021; 25: 100915

27. Mahesh A, Varma SVK, Raju CSK, Babu MJ, Animasaun IL, Nehad AS. Significance of Reynolds number, lower and upper rotating disks on the dynamics of water conveying grapheme and silver nanoparticles between rotating disks. *Physica Scripta.* 2021; 96: 045218.

28. Sowmya G, Gireesha BJ, Animasaun IL, Nehad AS. Significance of buoyancy and Lorentz forces on water-conveying iron(III) oxide and silver nanoparticles in a

rectangular cavity mounted with two heated fins: heat transfer analysis. *Journal of Thermal Analysis and Calorimetry*. 2021; 144: 2369–2384

29. Nehad AS, Animasaun IL, Chung JD, Wakif A, Alao FI, Raju CSK. Significance of nanoparticle's radius, heat flux due to concentration gradient, and mass flux due to temperature gradient: The case of Water conveying copper nanoparticles. *Scientific Reports*. 2021; 11:1882.

30. Thanaa E, Animasaun IL, Nehad AS. Ternary-hybrid nanofluids: significance of suction and dual-stretching on three-dimensional flow of water conveying nanoparticles with various shapes and densities. *Zeitschrift für Naturforschung A*. https://doi.org/10.1515/zna-2020-0317.

31. Nehad AS, Animasaun IL, Wakif A, Koriko OK, Sivaraj R, Adegbie KS, Zahra A, Vaidya H, Ijirimoye AF, Prasad KV. Significance of suction and dual stretching on the dynamics of various hybrid nanofluids: Comparative analysis between type I and type II models. *Physica Scripta*. 2020; 95:095205.

32. Bianco V, Manca O, Nardini S. Numerical investigation on nanofluids turbulent convection heat transfer inside a circular tube. *International Journal of Thermal Sciences.* 2209; 29: 3632-3642.

33. Mirmasoumi S, Behzadmehr A. Numerical study of laminar mixed convection of a nanofluid in a horizontal tube using two-phase mixture model. *Applied Thermal Engineering*. 2008; 28: 717-27.

34. Akbarinia A, Laur R. Investigation the diameter of solid particles effects on a laminar nanofluid flow in a curved tube using a two-phase approach. *International Journal Heat and Fluid Flow*. 2009; 30: 706-14.

35. Buongiorno J. Convective transport in nanofluids. *ASME J. Heat Transfer*. 2006; 128: 240-250.

36. Tzou DY. Instability of nanofluids in natural convection. *ASME J. Heat Transfer*. 2008; 128: 240-250.

37. Tzou DY. Thermal instability of nanofluids in natural convection. *Int. J Heat Mass Transfer.* 2008; 51: 2967-2979.

38. Hwang KS, Jang SP, Choi SUS. Flow and convective heat transfer characteristics of water-based Al_2O_3 nanofluids in fully developed laminar flow regime. *Int. J. Heat Mass Transfer*. 2009; 52: 193-199.

39. Nield DA, Kuznetsov AV. Thermal instability in a porous medium layer saturated by a nanofluid. *Int. J. Heat Mass Transfer*. 2009; 52: 5796-5801.

40. Prabhat N, Buongiorno J, Hu LW. Convective heat transfer enhancement in nanofluids: Real anomaly or analysis artifact? *Proc. the ASME/JSME 2011 8th Thermal Engineering Joint Conference, AJTEC201.* Honolulu, Hawaii, USA. 13-17 March 2011: 1-10.

41. Zhou XF, Gao L. Effective thermal conductivity in nanofluids of non-spherical particles with interfacial thermal resistance: differential effective medium theory. *J. Appl. Phys*. 2006; 100: 0249131-0249136

42. Gao L, Zhou XF. Differential effective medium theory for thermal conductivity in nanofluids. *Phys Lett A* . 2006; 348: 355-360.

43. Gao L, Zhou X, Ding Y. Effective thermal and electrical conductivity of carbon nanotube composites. *Chem. Phys Lett*. 2007; 434: 297-300.

44. Kim J, Choi CK, Kang YT, Kim MG. Effects of thermodiffusion and nanoparticles on convective instabilities in binary nanofluids. *Nanoscale Microscale Thermophys Eng*. 2006; 10: 29-39.

45. Nield DA, Kuznetsov AV. The effect of local thermal non-equilibrium on the onset of convection in a nanofluids. *ASME J. Heat Transfer*. 2010; 132: 052405-7.

46. Omid A, Rashidi S, Esfahani JA. Effects of perforated anchors on heat transfer intensification of turbulence nanofluid flow in a pipe. *J. of Thermal Analysis and Calorimentry*. 2020; 141: 2047–2059.

47. Shirejini SZ, Rashidi S, Esfahani JA. Recovery of drop in heat transfer rate for a rotating system by nanofluids. Journal of Molecular Liquids. 2016; 220: 961-969.

48. Rashidi S, Bovand M, Esfahani JA. Opposition of Magnetohydrodynamic and Al_2O_3 –water nanofluid flow around a vertex facing triangular obstacle. Journal of Molecular Liquids. 2016; 215: 276–284.

49. Rashidi S, Bovand M, Esfahani JA. Structural optimization of nanofluid flow around an equilateral triangular obstacle. Energy. 2015;30:1-14.

50. Bovanda M, Rashidi S, Ahmadib G, Esfahani JA. Effects of trap and reflect particle boundary conditions on particle transport and convective heat transfer for duct flow-A two-way coupling of Eulerian-Lagrangian ,odel. Applied Thermal Engineering. 2016; 100:39-54.

51. Maskaniyan M, Rashidi S, Esfahani JA. A two-way couple of Eulerian-Lagrangian model for particle transport with different sizes in an obstructed channel. *Powder Technology*. 2017;312:260-269.

52. Aung W, Worku G. Theory of fully developed, combined convection including flow reversal. *ASME J. Heat Transfer*. 1986; 108: 485-488.

53. Cheng C, Kou H, Huang W. Flow reversal and heat transfer of fully developed mixed convection in vertical channels. *AIAA J. Thermophys. Heat Transfer*. 1990; 4: 375-383.

54. Barletta A. Laminar mixed convection with viscous dissipation in a vertical channel. *Int. J. Heat Mass Transfer*. 1998; 41: 3501-3513.

55. Grosan T, Pop I. Thermal radiation effect on fully developed mixed convection flow in a vertical channel. *Tech. Mech*. 2007; 27: 37-47.

56. Javeri V. Simultaneous development of the laminar velocity and temperature fields in a circular duct for the temperature boundary condition of the third kind. *Int. J. Heat Mass Transfer* . 1976; 19: 943-949.

57. Zanchini E. Effect of viscous dissipation on mixed convection in a vertical channel with boundary conditions of the third kind. *Int. J. Heat Mass Transfer*. 1998; 41: 3949-3959.

58. Novy R, Davis H, Scriven L. A comparison of synthetic boundary conditions for continuous-flow systems. *Chem. Eng. Sci*. 1991; 46: 57-68.

59. Bixler N. Stability of a coating flow. *Diss. Abst. Int. B: Sci. Eng*. 1983; 43.

60. Papanastasiou T, Malamataris N, Ellwood K. A new outflow boundary condition. *Int. J. Numer. Methods Fluids*. 1992; 14: 587-608.

61. Pacheco-Vega J, Rodic RPT. A general scheme for the boundary conditions in convective and diffusive heat transfer with immersed boundary methods. *ASME International Mechanical Engineering Congress*, USA, 2006; 129: 5-10.

62. Umavathi JC, Bég OA. Numerical study of double-diffusive dissipative reactive convective flow in an open vertical duct containing a non-Darcy porous medium with Robin boundary conditions. *J. Engineering Mathematics*. 2019; 119: 135-147.

63. Umavathi JC, Bég OA. Mathematical modelling of triple diffusion in natural convection flow in a vertical duct with Robin boundary conditions, viscous heating and chemical reaction effects. *J. Engineering Thermophysics*. 2020; 29: 1–26.

64. Jaewook A, Jung I, Choi KK. Analysis of convective heat transfer in channel flow with arbitrary rough surface. *Z Angew Math Mech*. 2018; 1-19.

65. Togun *et al.*H. Thermal performance of nanofluid in ducts with double forward-facing steps. *Journal of the Taiwan Institute of Chemical Engineers*. 2015; 47: 28-42.

66. Reddy *et al.* YSK. Thermal energy analysis on liquid desiccant air conditioning system at different desiccant solution parameters. *Proceedings of the Institution of Mechanical Engineers, Part E: Journal of Process Mechanical Engineering*. 2020; 5: 1052-1065.

67. Jha *et al.,* BK. Steady fully developed mixed convection flow in a vertical parallel plate microchannel with bilateral heating and filled with porous material. *Proceedings of the Institution of Mechanical Engineers, Part E: Journal of Process Mechanical Engineering*. 2012; 227: 56-66.

68. Faizan *et al.* M. Implication of geometrical configuration on heat transfer enhancement in converging minichannel using nanofluid by two phase mixture model: A numerical analysis. *Proceedings of the Institution of Mechanical Engineers, Part E: Journal of Process Mechanical Engineering*. 2020. **In press**

69. Al Hairy M, Witery A. Heat transfer investigation in channel plate heat exchange. *Proceedings of the Institution of Mechanical Engineers, Part E: Journal of Process Mechanical Engineering*. 2007; 221: 101-107.

70. Rice RG, Do DC. *Applied Mathematics and Modelling for Chemical Engineers*, 2nd edn, John Wiley & Sons, New York. 2012.

71. Das SK, Choi SUS *et al*. *Nanofluids: Science and Technology*. CRC Press, Florida, USA. 2007.

72. Gebhart B *et al*. *Buoyancy-induced Flows and Transport*. Hemisphere, Washington, USA. 1988.

73. Bég OA, Khan MS, Karim I, Alam MM and Ferdows M. Explicit numerical study of unsteady hydromagnetic mixed convective nanofluid flow from an exponentially stretching sheet in porous media. *Applied Nanoscience.* 2014; 4: 943-957.

74. Thumma T, Bég OA, Kadir A. Numerical study of heat source/sink effects on dissipative magnetic nanofluid flow from a non-linear inclined stretching/shrinking sheet, *J. Molecular Liquids.* 2017; 232: 159-173.

75. Umavathi JC, Bég OA. Mathematical modelling of triple diffusion in natural convection flow in a vertical duct with Robin boundary conditions, viscous heating and chemical reaction effects. *J. Engineering* Thermophysics. 2020; 29: 1–26.

76. Bég OA, Motsa SS, Eemaan, Bég TA, Kadir A, Abbas AJ, Sohail A. Numerical study of nonlinear heat transfer from a wavy surface to a high permeability medium with pseudo-spectral and smoothed particle methods. *Int. J. Applied Computational Mathematics*. 2017; 3: 3593–3613.

77. Ko TH. Effects of corrugation angle on developing laminar forced convection and entropy generation in a wavy channel. *Heat Mass Transfer*. 2007; 44: 261–71.